

www.lpr-journal.org

High Stable Mechanoluminescence from TbBO₃ GCs for Stress Safety Monitoring

Jianqiang Xiao, Yiyu Cai, Yingdan Song, Haitao Tang, Pengfei Zhang, Qingpeng Peng, Xuhui Xu, Zhichao Liu,* and Lei Zhao*

Mechanoluminescence (ML) materials are widely used in information storage, stress sensing, and structural health monitoring due to their simplicity, nondestructiveness, and real-time sensing characteristics. However, the currently reported ML films suffer from high-temperature decomposition, opacity, and unstable ML properties, which seriously limits their applications. Herein, a transparent TbBO3 glass-ceramic (GCs) with significant ML performance is explored. A large number of Si-O and B-O tetrahedra in the glass matrix greatly improves the structural stability. Meanwhile, the disordered atomic arrangement reduces the obstacles in the light propagation process, making it highly transparent. Furthermore, femtosecond laser irradiation produces an ultra-deep trap of 517 K, which makes its ML performance highly stable. Based on this material, an aircraft stress safety monitoring system that can accurately pinpoint where the aircraft window is hit is designed. Therefore, this work provides a new strategy for the design of highly stable and transparent ML materials.

1. Introduction

Stress sensors have broad application prospects in human-computer interaction, wearable devices, and structural health monitoring.^[1] Traditional electronic stress sensors (such as piezoelectric, capacitive, and resistive detectors) mainly rely on the piezoelectric effects^[2] or piezoresistive effects,^[3] and are susceptible to electromagnetic field interference, making it difficult to ensure the stability of their operation.^[4] In addition, it requires

J. Xiao, Y. Cai, H. Tang, Q. Peng, X. Xu, Z. Liu

Faculty of Materials Science and Engineering

Yunnan Joint International Laboratory of Optoelectronic Materials and

Devices

Kunming University of Science and Technology

Kunming 650093, P. R. China E-mail: liuzhichzo1028@126.com

Y. Song, P. Zhang, L. Zhao

Baoji Key Laboratory of Micro-Nano Optoelectronics and Terahertz Technology

nology

School of Physics and Opto-Electronic Technology

Collaborative Innovation Center of Rare-Earth Optical Functional Materials and Devices Development

Baoji University of Arts and Sciences Baoji, Shaanxi 72 1016, P. R. China E-mail: zhaoleibjwl@ 163.com

The ORCID identification number(s) for the author(s) of this article can be found under https://doi.org/10.1002/lpor.202301002

DOI: 10.1002/lpor.202301002

additional power supply and signal processing systems, greatly increasing the complexity of the equipment.^[5] Compared with electronic stress sensors, stress sensors based on mechanoluminescent materials have emerged as a promising alternative for mechanical sensing. It can convert mechanical stimuli into optical parameters such as luminescence intensity,^[6] emission wavelength,^[7] and force-induced afterglow.^[8] Particularly, stress visualization is its greatest advantage.

So far, mechanoluminescence sensors have been widely used in areas such as human-computer interaction, [1b,9] signal control, [10] and mechanics imaging. [11] For example, Terasaki et al. successfully recorded local ML images of vehicles as they passed the bridge with a sensitive CCD camera by embedding SrAl₂O₄:

Eu²⁺ composite film into the cracks of the concrete bridge, recording.[12] Furthermore, Liu et al. proposed a bite-controlled photoelectric system that uses a distributed beam sensor driven by mechanical luminescence, integrated into a mouth guard, to enable control of computers, mobile phones, and wheelchairs.[10] Subsequently, Zhang et al. [9] also reported a composite film encapsulated with PDMS and $\mbox{Tb}_3\mbox{Al}_5\mbox{O}_{12}^{\mbox{-}}$: \mbox{Ce}^{3+} phosphor for robotic tactile sensing. Not surprisingly, most of the currently reported ML materials employ organic polymer matrices (e.g., PDMS, PMMA, SG) to encapsulate ML luminescent particles for ML detection.^[13] However, the encapsulated ML luminescent particles tend to be large and non-uniformly distributed within the organic polymer matrix, which results in low resolution and transparency. Meanwhile, the poor physical and chemical stability of organic composites limits their long-term stability, thereby restricting their potential application areas.

It is reported that amorphous is a traditional transparent medium^[14] with excellent high environmental stability^[15] and optical properties.^[16] Its excellent optical waveguide media has become an indispensable part of modern communication technology,^[17] leveraging the waveguide effect of light transmission within the glass to rapidly convey information. Compared to other transmission methods, optical signals exhibit high stability and secrecy because they are not affected by external electromagnetic fields.^[18] In addition, there are a large number of silicon-oxygen tetrahedral structures and boron-oxygen tetrahedra in glass, which makes it have high structural stability.^[19]

18638899, 2024, 3, Downloaded from https://onlinelibrary.wiley.com/doi/10.1002/por.202301002 by Kunning University Of, Wiley Online Library on [02/12/2024]. See the Terms and Conditions (https://onlinelibrary.wiley.com/terms-and-conditions) on Wiley Online Library for rules of use; OA articles are governed by the applicable Creative Commons License

www.lpr-journal.org

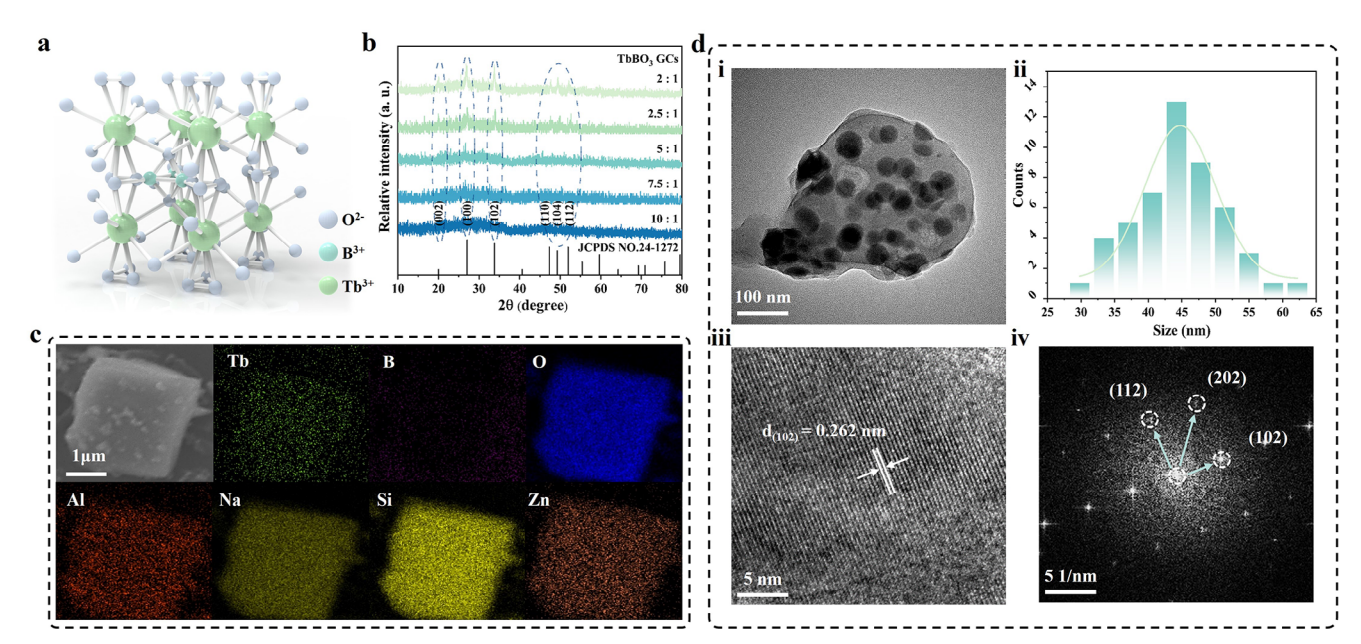


Figure 1. a) Crystal structure; b) XRD patterns of different mixing ratios (10:1, 7.5:1, 5:1, 2:5:1, 2:1); c) SEM image and elemental distribution; d) TEM image; particle size distribution histogram; HRTEM image and selected area electron diffraction (SAED) image.

Glass-ceramic is a composite material formed by glass and nanocrystals. It not only has a stable structure and high transparency of glass but also has excellent luminescence performance of nanocrystals.^[20] Therefore, these characteristics provide the possibility to explore the highly stable ML of glass ceramics.

In this work, TbBO₃ GCs were successfully synthesized by a two-step melt-quenching method. The results show that the TbBO₃ GCs have highly stable ML properties, and their ML intensity remains at more than 70% of the original even after 21 days of placement. This is due to the ultra-deep trap at 517 K created by femtosecond laser (800 nm) irradiation. In addition, it also has good environmental stability and high transparency. Therefore, we designed a stress safety monitoring system for aircraft windshield windows with this material, which can determine the location of damage in real-time. This work will open up a new path for the development of high-transparency and high-stability real-time stress sensors.

2. Results and Discussion

TbBO₃ GCs are synthesized by a two-step melt quenching method, and the crystal phase and microstructure of the samples are shown in **Figure 1**. TbBO₃ belongs to the hexagonal crystal system with a space group of P6₃/mmc. The Tb³⁺ ion is situated within a 14-hadron coordination environment, resulting from the coordination of twelve oxygen ions. Conversely, the B³⁺ ion occupies a trigonal planar coordination environment, formed by the coordination of three oxygen ions, as depicted in Figure 1a,b displays the X-ray diffraction (XRD) patterns of TbBO₃ GCs samples prepared with different mixing ratios (M precursor glass: M phosphor). It can be found that all diffraction peaks are in good agreement with the standard card of TbBO₃ (JCPDS No. 24–1272), indicating that the samples are pure phase. Additionally, LuBO₃ GCs

and YBO3 GCs samples were prepared simultaneously in order to verify the feasibility of the two-step melt quenching method for the preparation of borate GCs. The XRD patterns of these samples (Figure S1, Supporting Information) also agree well with the standard card, further demonstrating the wide applicability of the two-step melt-quenching method in the synthesis of borate GCs. Figure 1c gives the SEM image and element mapping of borate GCs, the Tb, B, O, Al, Na, Si, and Zn elements are uniformly distributed in the sample. TEM image of borate GCs in Figure 1d shows that TbBO3 nanocrystals (NCs) are precipitated in the enclosed in an amorphous matrix with an average diameter of \approx 44.58 nm. In addition, the high-resolution field transmission electron microscopy (HRTEM) image presents a clear 1D lattice spacing at 0.262 nm, which is consistent with the (102) plane of TbBO3. The corresponding selected area electron diffraction (SAED) image further classifies these precipitated NCs as TbBO₃

The photoluminescence (PL) and PL excitation (PLE) spectra of TbBO₃ GCs are shown in Figure 2a. It can be seen that there are four emission peaks at 488, 546, 584, and 620 nm when excited at 376 nm, which are attributed to the ⁵D₄-⁷F₆, ⁵D₄-⁷F₅, ⁵D₄-⁷F₄ and ⁵D₄-⁷F₃ transitions of Tb³⁺ ions, respectively.^[21] A bright green luminescence can be detected under UV (365 nm) excitation, presented in the inset of Figure 2a, which confirms that TbBO3 GCs have a high luminosity. Furthermore, the excitation bands ≈265 and 376 nm in the PLE spectrum of TbBO₃ GCs are attributed to the f-d and f-f transitions of Tb³⁺ ions, respectively. Figure 2b gives the CIE coordinates of TbBO3 GCs, and the coordinate values are (0.3433, 0.5833), which further confirms that TbBO₃ GCs have a green emission. As the mixing ratio (M $_{\rm precursor\,glass}$: M $_{\rm phosphor}$) increases, the green emission intensity gradually increases, as depicted in Figure 2c,d, while the transparency of TbBO₃ GCs gradually decreases until devitrification, which is mainly due to the formation of more TbBO₃ NCs.

18638899, 2024, 3, Downloaded from https://onlinelibrary.wiley.com/doi/10.1002/por.202301002 by Kunning University Of, Wiley Online Library on [02/12/2024]. See the Terms and Conditions (https://onlinelibrary.viley.com/erms-and-conditions) on Wiley Online Library of use; OA arctles are governed by the applicable Creative Commons License

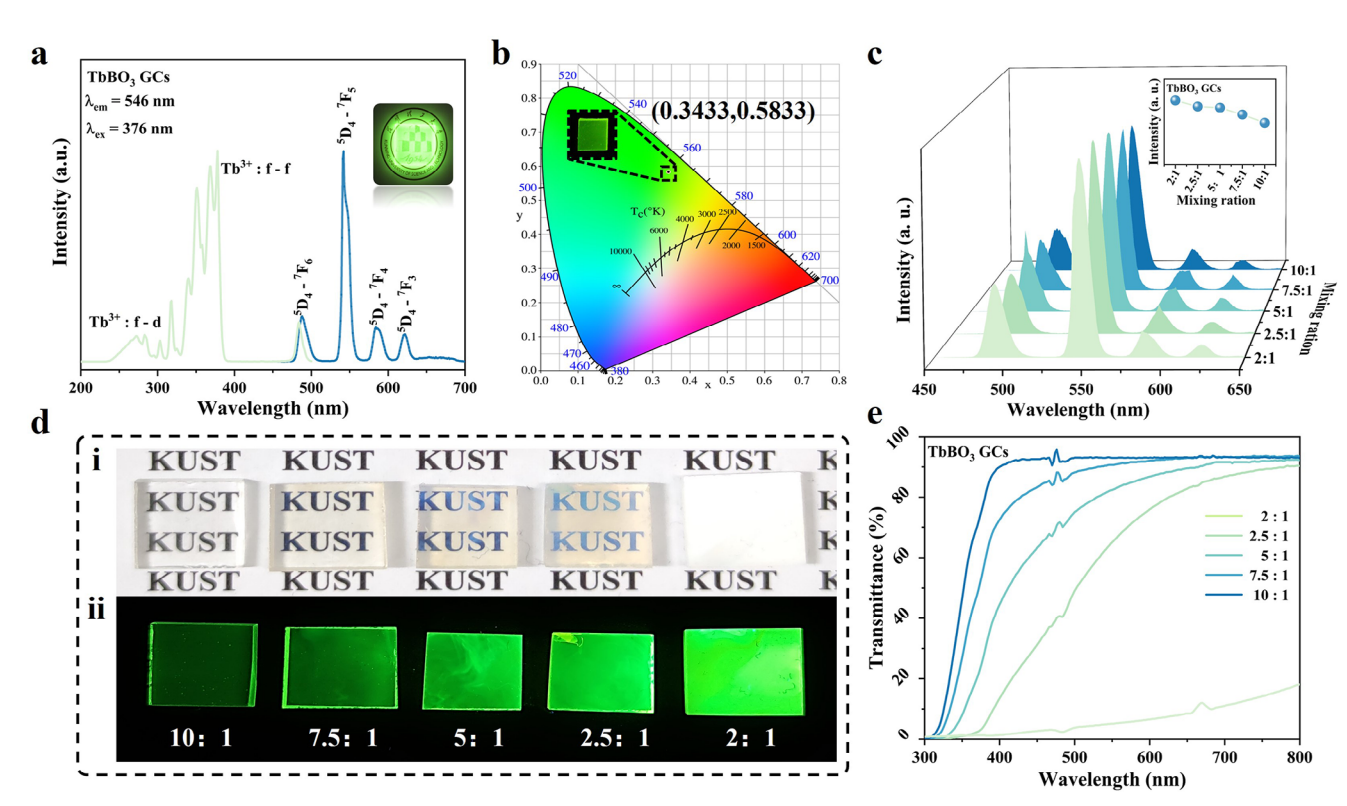


Figure 2. a) PLE and PL spectra of TbBO₃ GCs; the inset shows an optical photo of TbBO₃ GCs under the irradiation of a 365 nm UV lamp; b) CIE chromaticity coordinates of TbBO₃ GCs (inset is a photo of luminescence at 365 nm UV lamp); c) PL spectra of TbBO₃ GCs at different doping ratios (10:1, 7.5:1, 5:1, 2.5:1, 2:1); the inset depicts PL intensity versus doping ratios; d) Photos of different doping ratios under sunlight and 365 nm UV lamp; e) Transmission spectra of TbBO₃ GCs at different doping ratios.

Figure 2e presents the change of transmittance with an increasing mixing ratio. Obviously, with the increase of the mixing ratio, the transmittance gradually decreases, which is consistent with the transparency photograph in Figure 2d.

The femtosecond (fs) laser irradiation could instantly nonlinear optical effects in glasses by photon-matter interaction, owning to an ultrahigh instantaneous power.^[22]

A bright green ML is observed in TbBO₃ GCs after fs laser irradiation as presented in Figure 3a and Video S1 (Supporting Information), and the ML spectrum of the TbBO₃ GCs shows the same emission center as that of PL. Figure 3b displays the ML photo and ML dimension color image of TbBO₃ GCs in the dark and sunlight. Interestingly, even in sunlight, clear ML phenomena can also be captured by the naked eye or CCD camera. To clarify the origin of the ML, the TL curves of TbBO₃ GCs before and after fs laser irradiation are compared in Figure 3c. Two distinct TL peaks can be observed at 423 and 517 K, indicating that there are two depths of traps in TbBO₃ GCs after fs laser irradiation.

The trap depth can be calculated by utilizing the following approximate equation as follows^[23]:

$$E (eV) = \left(\frac{T_{M}}{500}\right) \tag{1}$$

where the thermally active energy *E* (eV) at the depth of the trap represents the energy gap between the electron trap and the con-

duction band, $T_{\rm M}$ (K) is the location of the TL peak temperature. Therefore, the trap depths of this different TL peak can be calculated from the above equation as 0.846 and 1.034 eV, respectively. Figure 3d shows the EPR curves of the TbBO₃ GCs sample before and after fs laser irradiation. Compared with the EPR before fs laser irradiation, an obvious EPR signal is observed \approx g = 1.997 after fs laser irradiation. It is attributed to the nonbridging oxygen vacancy centers in the glass after fs laser irradiation.[24] Here, a schematic diagram of the principle for generating ML is presented in Figure 3e. fs laser-induced nonbridge oxygen bond of the glass matrix is broken with the formation of trapping centers. Moreover, free electrons and holes are formed in the glass matrix through multiphoton ionization, Joule heating, and collisional ionization processes, which could be trapped by the trapping center. Then mechanical stimulation is applied, and Joule heat is generated through work between the force-exerting object and the sample, which in turn stimulates the release of carriers in the trap, and transfers the released energy to the emission center of the Tb³⁺ ions, producing a bright green ML.

To further explore the influencing factors of ML properties, the ML spectra of TbBO₃ GCs with different mixing ratios after fs laser irradiation are shown in **Figure 4a**, and the ML photos with different mixing ratios under 10 N are presented in Figure S2 (Supporting Information). The results show that the ML intensity increased with the increase of the mixing ratio, but the transparency gradually decreased. Considering the two influencing factors of ML intensity and transparency, the sample with a

18638899, 2024, 3, Downloaded from https://onlinelibtary.wiley.com/doi/10.1002/lpor.202301002 by Kunning University Of, Wiley Online Library on [02/12/2024]. See the Terms and Conditions (https://onlinelibrary.wiley.com/erms-and-conditions) on Wiley Online Library for nules of use; OA arcicles are governed by the applicable Creative Commons Licensea

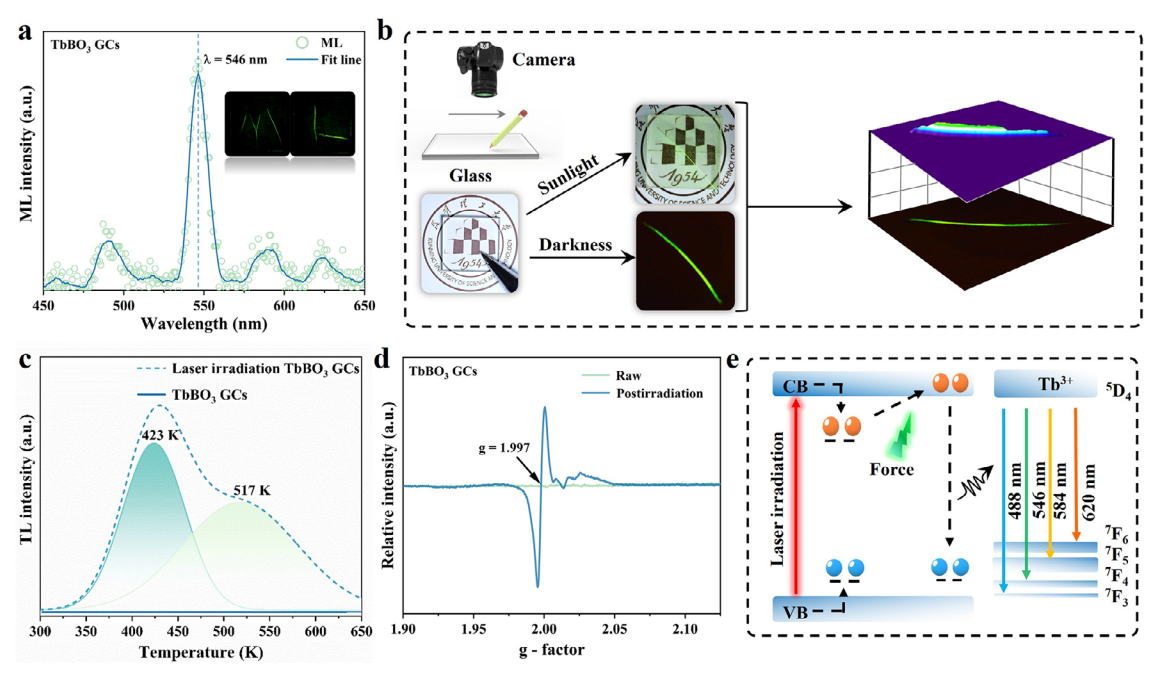


Figure 3. a) ML spectrum of TbBO₃ GCs; b) ML photo and dimensional color image under sunlight and dark conditions; c) TL curves (dotted line) and two fitted peaks (solid line) d) EPR curves of TbBO₃ GCs before and after fs laser irradiation; e) Mechanism proposed for mechanical-to-optical energy conversion of TbBO₃ GCs.

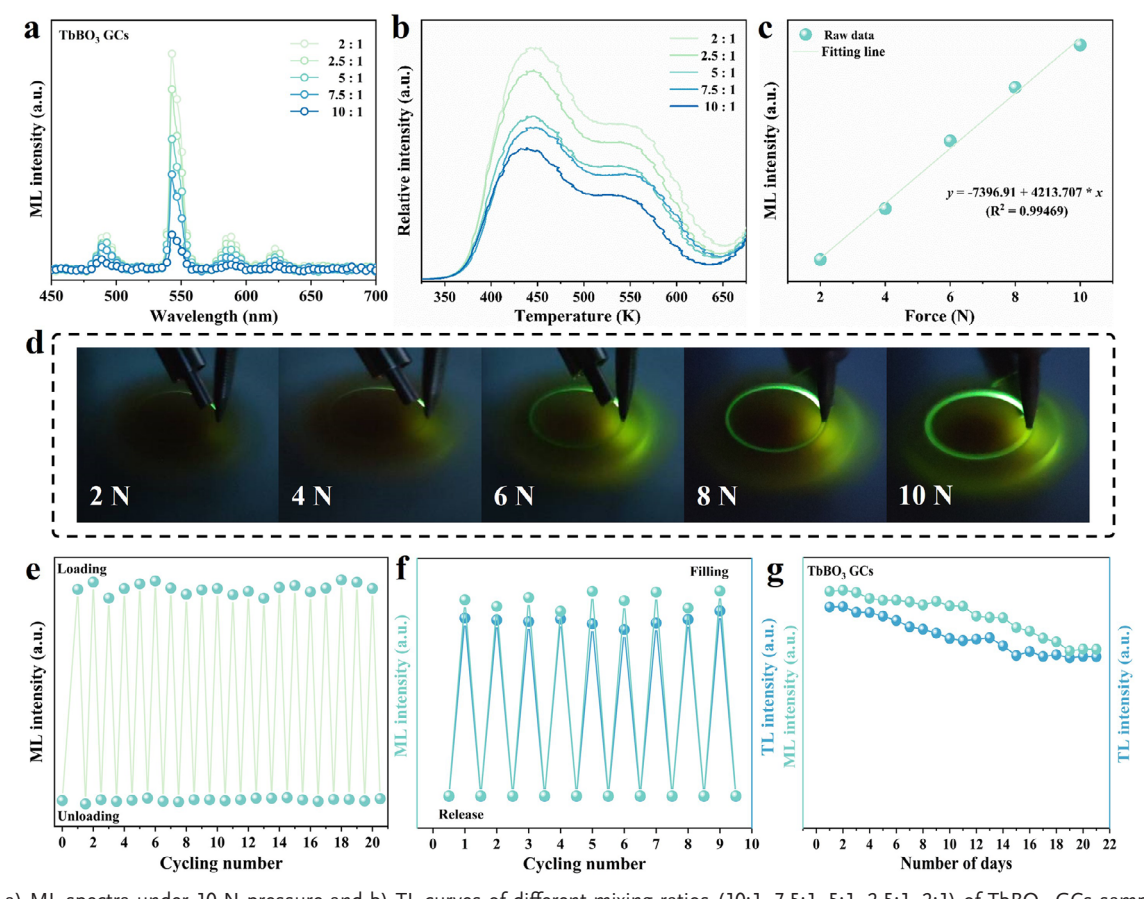


Figure 4. a) ML spectra under 10 N pressure and b) TL curves of different mixing ratios (10:1, 7.5:1, 5:1, 2.5:1, 2:1) of TbBO₃ GCs samples; c) ML intensity of TbBO₃ GCs under different pressures and d) ML photograph; e) ML intensity for 21 cycles of force loading and unloading after fs laser filling at beginning; f) ML and TL intensity after 10 cycles of fs laser filling and thermal removal; g) ML and TL intensity after 21 days storage.

18638899, 2024, 3, Downloaded from https://onlinelibrary.wiley.com/doi/10.1002/por.202301002 by Kunning University Of, Wiley Online Library on [02/12/2024]. See the Terms and Conditions (https://onlinelibrary.wiley.com/terms-and-conditions) on Wiley Online Library for rules of use; OA articles are governed by the applicable Creative Commons License

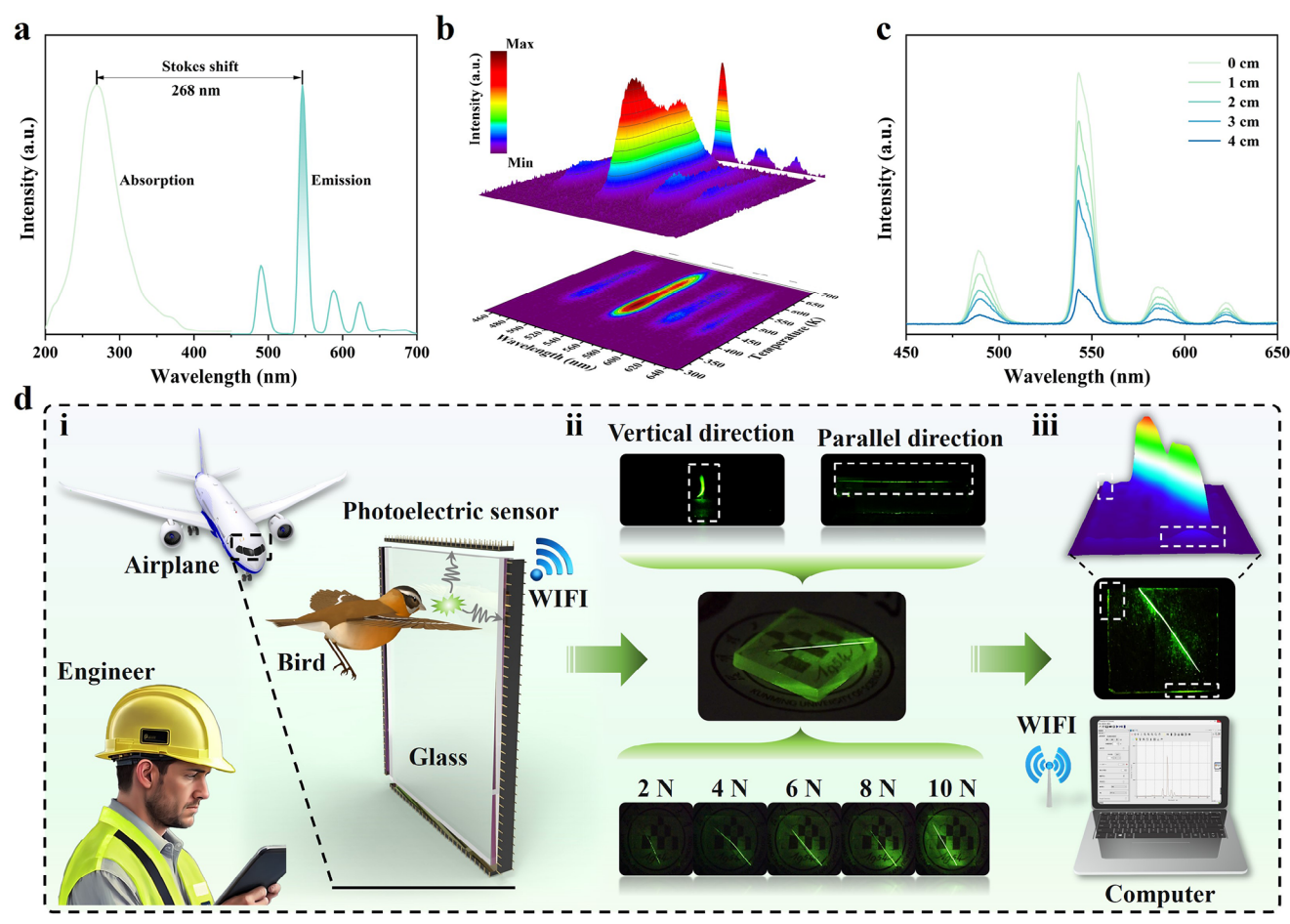


Figure 5. a) Absorption and PL spectra of TbBO₃ GCs; b) 3D TL spectra; c) ML spectra at different distances from the glass edge; d) Schematic diagram of application to stress safety monitoring of aviation aircraft.

mixing ratio of 2.5:1 was selected for subsequent testing. In addition, TL curves of TbBO $_3$ GCs with different mixing ratios after fs laser irradiation have a similar changing trend with the ML intensity. Here, we designed a stress detection optical system, as shown in Figure S3a,b (Supporting Information). The force is adjusted by changing the mass of the weight, and the stress signal is collected with a fiber optic spectrometer. The relationship between ML intensity and the applied force of TbBO₃ GCs is tested, as shown in Figure 4c. It can be seen that the ML intensity has a linear relationship with the magnitude of the applied force, indicating the TbBO₃ GCs have good stress-sensing properties. Figure 4d gives the ML photos corresponding to different applied forces (2-10 N) after fs laser irradiation, and the ML brightness increased with the application load. Moreover, ML intensity recovery of the TbBO3 GCs is tested, as shown in Figure 4e. After 21 cycles of force application, the ML intensity remained almost unchanged at more than 90% of the original intensity. Owing to the positive relationship between the ML and TL, ML, and TL reproducible properties of TbBO3 GCs after fs laser fillings and thermal clearing are measured in Figure 4f, which prove that ML and TL of TbBO3 GCs have good cycling stability and good correlation. Interestingly, after 21 days of storage, the ML and TL intensity of TbBO₃ GCs samples still have more than 70% of the

original intensity after fs laser irradiation, as shown in Figure 4g. It is attributed to the carriers in deep traps are difficult to release under thermal perturbation at room temperature.

Compared to ML thin film, TbBO₃ GCs with high transparency and optical waveguide effect have an absolute advantage in practical application, as shown in Figure S4 (Supporting Information), which has been verified in the above statement. Especially, The TbBO3 GCs sample we prepared has a transmittance of more than 80% and a large stokes shift of 268 nm (Figure 5a). The absence of overlap between the absorption and emission spectra indicates that TbBO₃ GCs have zero self-absorption, which is extremely favorable for the optical waveguide effect. At the same time, considering that the device we designed may be exposed to sunlight in daily life, the 3D TL spectra of TbBO3 GCs are measured in Figure 5b. It can be seen that although the emission intensity decreases slightly with the increasing temperature, the peak position hardly changes, which can effectively ensure the quality of signal transmission. As shown in Figure S5 (Supporting Information), TbBO3 GCs samples were soaked in air, water, and alcohol for up to 10 h, and the PL intensity of TbBO₃ GCs hardly changed. considering that the glass medium will cause loss of the optical signal, for the spectra with increasing distance from the ML source to the glass boundary, ML intensity as well as the full width at half maximum (FWHM) are tested with the same load, depicted in Figure 5c and Figure S6a,b (Supporting Information), respectively. It can be found that the ML intensity decreased linearly with increasing distance, while the peak position and FWHM did not change. These results prove that the weakening of the optical signal comes from the loss of the medium rather than the self-absorption of the fluorescent particles. Based on the ML intensity decreasing linearly with the increase of distance is beneficial to the precise localization of ML sites, we designed a stress detection device applied to the front windshield of the cockpit of an aviation aircraft. When birds or flying objects hit the front windshield, an ML signal is generated, which is transmitted to the edge of the front windshield through the optical waveguide effect and collected by the optical signal collector. Thereafter, the signal is fed back to the flight attendant's computer or mobile phone through wireless transmission, and the flight attendants can determine the location of the impact based on the magnitude of the signal. Meanwhile, we also simulate this situation with the TbBO_3 GCs we prepared, as presented in the inset of Figure 5d. When a hard object hits the TbBO3 GCs, a clear green glow can be seen from the edge of the TbBO3 GCs, which further illustrates the possibility of our fabricated TbBO₃ GCs for long-range mechanical detection applications.

3. Conclusion

In summary, the highly transparent TbBO₃ GCs with stable structure and excellent ML performance were synthesized by two melt quenching methods. After fs laser irradiation, it can produce ultra-deep traps with a depth of 517 K, which is extremely stable under thermal disturbance at room temperature. More than 70% of the original ML intensity remained after 21 days of placement. When placed in air, water, and alcohol for 10 h, the luminescence intensity hardly changes. In addition, due to the large Stokes shift, the TbBO₃ GCs have almost no self-absorption during the optical waveguide, which further ensures the accuracy of their stress-generating position capture. This work not only opens up a new path for real-time crack monitoring of aircraft windshields but also provides new ideas for the next generation of visual stress tracking.

4. Experimental Section

Sample Synthesis: The precursor glass (PG) of $51B_2O_3$ - $28SiO_2$ - $4ZnO_17Na_2CO_3$ (in mol%) was prepared by melt-quenching technique. B_2O_3 (99.99%), SiO_2 (99.99%), ZnO (99.9%), and Na_2CO_3 (99.99%) as raw materials were ground to a powder in an agate mortar. The stoichiometric compound was then placed in an alumina crucible and melted at 1200 °C for 30 min in the air atmosphere. Then, the melt was poured onto a copper plate preheated at 450 °C, pressed with another copper plate to form a precursor glass, and the obtained glass was ground into glass powder with a spherical mill.

 $Tb_3Al_5O_{12}$ phosphor was synthesized of by the high-temperature solid-phase method. Tb_4O_7 (99.5%), and Al_2O_3 (99.99%) as raw materials were mixed in a molar ratio in an agate mortar with some ethanol as cosolvent, and grind for 20 min. Then, the mixture was put into an alumina crucible and sintered in an electric furnace at 1600 °C for 510 min. After cooling the room temperature, the samples were pulverized in a ceramic mortar.

The PG powder and phosphor powder were mixed in an agate mortar in proportion, the mixture was then charged into an alumina crucible and

melted in the air at 1200 °C for 30 min. Then, pouring the melt onto a copper plate preheated at 450 °C, and pressing another copper plate to form TbBO $_3$ GCs, annealed in a muffle furnace at 400°C for 8 h to release thermal stress. Finally, the obtained TbBO $_3$ GCs product was cut, polished, or ground into powder for further characterization.

Characterization: XRD patterns were acquired using an X-ray diffractometer (D2 PHASER) with Ni-filtered Cu K α radiation. The PL and PLE spectra were determined by the FLS980 fluorescence spectrophotometer which was equipped with a 450 W Xe light source and dual excitation monochromators. The microstructure of the TbBO₃ GCs was analyzed by TEM and HRTEM using JEM-F200 operating at 200 KV. The powder morphology was observed using a scanning electron microscope (SEM) (JEOL JSM-6490). EDS (Energy Dispersive Spectrometer) measurements were carried out using an EDAX Apollo X SDD EDX detector. The transmittance and absorption spectra were recorded using a Model HITACHI U-4100 type spectrophotometer (Hitachi, Tokyo, Japan) over the spectral range of 200 to 800 nm. The thermoluminescence (TL) curves were collected using an FJ-427A TL meter (Beijing Nuclear Instrument Factory, Beijing, China). Electron paramagnetic resonance (EPR) spectra were measured using an EPR spectrometer (Bruker X-band A300 - 6/1) at room temperature near 9.2 GHz. The mechanical behavior was carried out using a friction testing machine (MS-T3001) and the ML signals were collected in situ via a fiber spectrometer (QE Pro, Ocean Optics). All photographs were taken with a digital camera (Nikon D7100) at room temperature.

Supporting Information

Supporting Information is available from the Wiley Online Library or from the author.

Acknowledgements

This work was financially supported by the National Natural Science Foundation of China (12364044), Yunnan Major Scientific and Technological Projects (202202AG050004, 202202AG050016), the International Joint Innovation Platform of Yunnan Province (202203AP140004), Science and Technology Talents and Platform Program (Workstation for academicians and Experts) (202205AF150005), Yunnan Provincial Natural Science Foundation (202001AS070008 and 202101AT070126), Yunnan Ten Thousand Talents Plan Young & Elite Talents Project (YNWR-QNBJ-2018-295), and Rare and Precious Metal Materials Genome Engineering Project of Yunnan Province (202002AB0800001).

Conflict of Interest

The authors declare no conflict of interest.

Data Availability Statement

The data that support the findings of this study are available on request from the corresponding author. The data are not publicly available due to privacy or ethical restrictions.

Keywords

high transparency, Mechanoluminescence, safety monitoring, stable structure

Received: October 6, 2023 Revised: November 15, 2023 Published online: December 12, 2023 18638899, 2024, 3, Downloaded from https://onlinelibrary.wiley.com/doi/10.1002/por.202301002 by Kunning University Of, Wiley Online Library on [02/12/2024]. See the Terms and Conditions (https://onlinelibrary.wiley.com/terms-and-conditions) on Wiley Online Library for rules of use; OA articles are governed by the applicable Creative Commons License

18638899, 2024, 3, Downloaded from https://onlinelibrary.wiley.com/doi/10.1002/por.202301002 by Kunning University Of, Wiley Online Library on [02/12/2024]. See the Terms and Conditions (https://onlinelibrary.wiley.com/terms-and-conditions) on Wiley Online Library for rules of use; OA

- a) D. J. ACS Energy LettersLipomi, M. Vosgueritchian, B. C. K. Tee, S. L. Hellstrom, J. A. Lee, C. H. Fox, Z. Bao, Nat. Nanotechnol. 2011, 6, 788; b) N. Li, S. Yu, L. Zhao, P. Zhang, Z. Wang, Z. Wei, W. Chen, X. Xu, Inorg. Chem. 2023, 62, 2024; c) C. Pang, G.-Y. Lee, T.-I. Kim, S. M. Kim, H. N. Kim, S.-H. Ahn, K.-Y. Suh, Nat. Mater. 2012, 11, 795; d) L. Liu, C. N. Xu, A. Yoshida, D. Tu, N. Ueno, S. Kainuma, Adv. Mater. Technol. 2018, 4, 1800336.
- [2] M. Xie, Y. Zhang, M. J. Krasny, C. Bowen, H. Khanbareh, N. Gathercole, Energy Environ. Sci. 2018, 11, 2919.
- [3] S. Lee, A. Reuveny, J. Reeder, S. Lee, H. Jin, Q. Liu, T. Yokota, T. Sekitani, T. Isoyama, Y. Abe, Z. Suo, T. Someya, *Nat. Nanotechnol.* 2016. 11, 472.
- [4] E. Vorathin, Z. M. Hafizi, N. Ismail, M. Loman, Opt. Laser Technol. 2020, 121, 105841.
- [5] N. Ni, C. C. Chan, W. C. Wong, L. Y. Shao, X. Y. Dong, P. Shum, Sens. Actuator A-Phys. 2010, 158, 207.
- [6] H. Liang, Y. He, M. Chen, L. Jiang, Z. Zhang, X. Heng, L. Yang, Y. Hao, X. Wei, J. Gan, Z. Yang, Adv Intell Syst 2021, 3, 2100035.
- [7] H. Bai, S. Li, J. Barreiros, Y. Tu, C. R. Pollock, R. F. Shepherd, *Science* 2020, 370, 848.
- [8] Y. Bai, X. Guo, B. Tian, Y. Liang, D. Peng, Z. Wang, Adv. Sci. 2022, 9, 2203249
- [9] P. Zhang, J. Wu, L. Zhao, Z. Guo, H. Tang, Z. Wang, Z. Liu, W. Chen, X. Xu, ACS Sustainable Chem. Eng. 2023, 11, 4073.
- [10] B. Hou, L. Yi, C. Li, H. Zhao, R. Zhang, B. Zhou, X. Liu, Nat. Electron. 2022, 5, 682.
- [11] S. Yu, S. Fang, L. Zhao, Y. Bai, R. Wang, Z. Wang, Chem. Eng. J. 2023, 474, 145542.
- [12] T. Kundu, N. Terasaki, C.-N. Xu, C. Li, L. Zhang, C. Li, D. Ono, M. Tsubai, Y. Adachi, Y. Imai, N. Ueno, T. Shinokawa, *Proc. SPIE* 2012, 8348. 83482D.
- [13] a) Y. Bai, F. Wang, L. Zhang, D. Wang, Y. Liang, S. Yang, Z. Wang, Nano Energy 2022, 96, 107075; b) Y. Yan, S. Fang, Y. Li, Y. Xu, Y. Song, Z. Ma, Y. Shi, L. Zhao, Z. Wang, J. Mater. Chem. C 2023, 11, 11509; c) Y. Song, Y. Li, Z. Chen, G. Zhang, A. N. Yakovlev, T. Hu, T. G. Cherkasova, X. Xu, L. Zhao, Ceram. Int. 2023, 49, 30685; d) X. Wang, M. Que, M. Chen, X. Han, X. Li, C. Pan, Z. L. Wang, Adv. Mater. 2017, 29, 1605817; e) Y. Du, Y. Jiang, T. Sun, J. Zhao, B. Huang, D. Peng, F. Wang, Adv. Mater. 2018, 31, 1807062; f) P. Xiong, B. Huang, D. Peng, B. Viana, M. Peng, Z. Ma, Adv. Funct. Mater. 2021, 31, 2010685.
- [14] a) H. Tang, Z. Liu, H. Zhang, X. Zhu, Q. Peng, W. Wang, T. Ji, P. Zhang, Y. Le, A. N. Yakovlev, J. Qiu, G. Dong, X. Yu, X. Xu,

- Adv. Opt. Mater. 2023, 11, 2300445; b) X. Huang, Q. Guo, D. Yang, X. Xiao, X. Liu, Z. Xia, F. Fan, J. Qiu, G. Dong, Nat. Photonics 2019, 14, 82; c) Z. Fang, H. Tang, Z. Yang, H. Zhang, Q. Peng, X. Yu, D. Zhou, J. Qiu, X. Xu, Adv. Opt. Mater. 2021, 9, 2101607.
- [15] Q. Huang, W. Chen, X. Liang, C. Lv, W. Xiang, ACS Sustainable Chem. Eng. 2023, 11, 9773.
- [16] a) C. Quan, X. Xing, S. Huang, M. Jin, T. Shi, Z. Zhang, W. Xiang, Z. Wang, Y. Leng, *Photonics Res* 2021, 9, 1767; b) H. Zhao, Y. Cun, X. Bai, D. Xiao, J. Qiu, Z. Song, J. Liao, Z. Yang, *ACS Energy Lett.* 2022, 7, 2060; c) G. Du, S. Wen, J. Zhao, P. Ran, D. Wang, L. Wei, X. Qiao, Y. Yang, J. Qiu, S. Zhou, *Adv. Mater.* 2023, 35, 2205578; d) M. Ouyang, H. Zhang, M. Li, J. Zhang, Y. Gong, X. Huang, X. Liu, J. Qiu, Z. Yang, G. Dong, *Laser Photon. Rev.* 2023, 17, 2300068; e) Z. Hu, X. Huang, Z. Yang, J. Qiu, Z. Song, J. Zhang, G. Dong, *Light Sci Appl* 2021, 10, 140.
- [17] a) R. D. MAURER, Glass fibers for optical communications, IEEE, New York City, US 1973 pp 452–462; b) W. C. Wang, B. Zhou, S. H. Xu, Z. M. Yang, Q. Y. Zhang, Prog. Mater. Sci. 2019, 101, 90
- [18] F. Song, A. J. Xie, S.-W. Seo, J Opt 2014, 16, 015503.
- [19] a) A. Herrmann, G. Völksch, D. Ehrt, Int J Appl Glass Sci 2019, 10, 532;
 b) M. A. Zeed, A. Saeed, R. M. El Shazly, H. M. El- Mallah, E. Elesh, Optik 2023, 272, 170491.
- [20] a) Q. Wang, M. Jin, Y. Chen, Y. Zhao, Y. Tong, Z. He, X. Liang, W. Xiang, Adv. Opt. Mater. 2021, 9, 2101518; b) J. Lin, Y. Lu, X. Li, F. Huang, C. Yang, M. Liu, N. Jiang, D. Chen, ACS Energy Lett. 2021, 6, 519; c) K. Sun, D. Tan, J. Song, W. Xiang, B. Xu, J. Qiu, Adv. Opt. Mater. 2021, 9, 2100094.
- [21] Z. Liu, L. zhao, X. Yang, L. Yang, H. zhang, W. zeng, X. Yu, J. Qiu, X. Xu, Chem. Eng. J. 2020, 401, 126119.
- [22] Q. Peng, T. Wang, H. Tang, T. Ji, W. Wang, J. Xiao, X. Li, Z. Liu, J. Qiu, X. Yu, X. Xu, Laser Photon. Rev. 2022, 16, 2100726.
- [23] a) N. S. M. Viswanath, G. K. Grandhi, H. J. Kim, Y. Zhuang, R.-J. Xie, W. B. Im, Appl. Mater. Today 2020, 18, 100518; b) C. Wang, Y. Jin, Y. Lv, G. Ju, D. Liu, L. Chen, Z. Li, Y. Hu, J. Mater. Chem. C 2018, 6, 6058; c) H. Guo, Y. Wang, G. Li, J. Liu, P. Feng, D. Liu, J. Mater. Chem. C 2017, 5, 12090.
- [24] a) H. Tang, L. Zhao, Z. Liu, Q. Peng, X. Yu, Q. Wang, F. Zhao, M. Deng, Y. Bai, Z. Wang, T. Wang, J. Qiu, X. Xu, Cell Rep Phys Sci 2022, 3, 101093; b) J. Ueda, A. Hashimoto, S. Tanabe, J. Phys. Chem. C 2019, 123, 29946.

articles are governed by the applicable Creative Commons I